Confinement of picosecond timescale current pulses by tapered coplanar waveguides

N. Peters,[1,2] M. Rosamond,[1] L. Li,[1] E. H. Linfield,[1] A. G. Davies,[1] M. Ali,[2] B. J. Hickey,[2] and J. Cunningham[1,a)]

[1]*School of Electronic and Electrical Engineering, University of Leeds, Woodhouse Lane, Leeds, LS2 9JT, United Kingdom*
[2]*School of Physics and Astronomy, University of Leeds, Woodhouse Lane, Leeds, LS2 9JT, United Kingdom*

Tapered coplanar waveguides with integrated photoconductors were designed, fabricated, and measured, with pulsed transmission results comparing well with High Frequency Structure Simulator simulations which predict increased confinement and electric field concentration in the tapered region. Devices made with titanium/gold metallisation were used to demonstrate transmission and confinement, while the magnetoresistive properties of devices with cobalt/copper multilayers were used to demonstrate the field concentration. In the latter case, a mathematical framework was developed to understand the relationship between tapering effects and the picosecond magnetoresistance response. © 2018 Author(s). All article content, except where otherwise noted, is licensed under a Creative Commons Attribution (CC BY) license (http://creativecommons.org/licenses/by/4.0/). https://doi.org/10.1063/1.5027202

The meV photon energies exhibited by terahertz (THz) frequency radiation (0.1–10 THz) are comparable with the energy spacings in a wide range of sub-micron-scale condensed matter systems. The most common approach to accessing the THz properties of such systems is via free-space THz time domain spectroscopy. Although previously best suited to the measurement of ensembles of small systems, recent modifications of the technique to provide near-field microscopy with broadband spectral coverage have been demonstrated, in which the THz radiation is restricted and/or focused by means of either apertures[1] or metallic tips,[2] for example. An alternative technique we developed embeds the object under study in a coplanar waveguide (CPW) with integrated photoconductors for THz-bandwidth signal excitation and detection. We have previously used this to investigate the plasmonic spectra of two-dimensional electron gases, for example.[3,4] Such geometries offer the advantage of precise lithographically defined control of an electric field placement[5] removing alignment problems associated with a scanned probe. Here, we demonstrate that tapering of the CPW can be used to enhance the THz field confinement further. We use this enhanced concentration of electric field to increase interaction with a magnetic multilayered system which exhibits giant magnetoresistance. The field enhancement induces a factor of ∼2.4 increase in the change in current with the magnetic field in the tapered waveguide relative to untapered THz CPWs.

An Ansoft High Frequency Structure Simulator (HFSS)[6] was first used to investigate the effects of tapering on the THz electric field confinement within a metallic CPW device [Fig. 1(a)]. The centre track of the coplanar waveguide in this simulation had a width of 30 μm, with a centre-conductor spacing of 10 μm between the centre track and the neighbouring ground planes. The ratio of the gap-width to the centre conductor width was then maintained as the CPW was tapered linearly to a centre conductor width of 1 μm with a gap of 0.33 μm over the course of 500 μm. Following simulation, cross-sections of the maximum instantaneous electric field strength (at 1 THz) were taken at intervals both going into and out of the tapered region [Fig. 1(a)]. From each cross-section, the field confinement and the average field strength in the confined region were extracted. For the
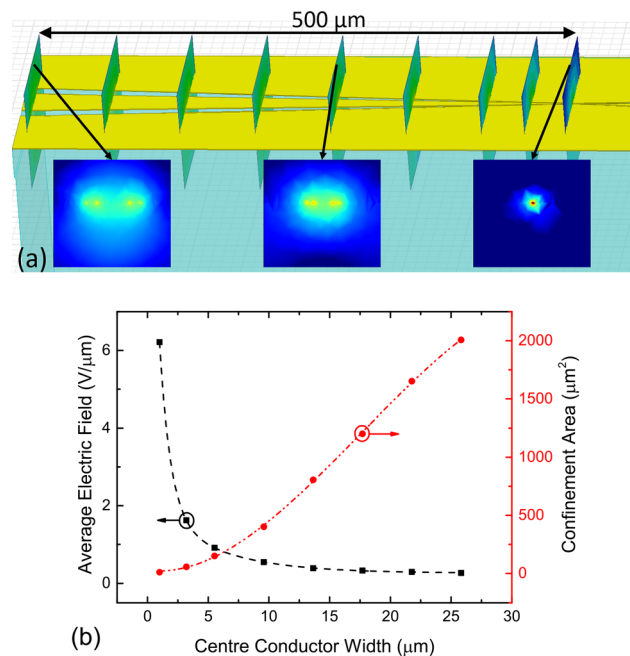
FIG. 1. (a) The HFSS model used to investigate the effect of tapering in CPWs. Cross-sections of the electric field at the start, middle, and end of the tapered region are shown in insets. (b) The confinement area and average instantaneous field strength of the CPW (at 1 THz) as a function of centre conductor width. The increase in the confinement (decrease in the confinement area) with the decreasing width corresponds to an increase in the average field strength. Dashed/dotted lines are guides for the eye.

a)Author to whom correspondence should be addressed: j.e.cunningham@leeds.ac.uk

112, 181103-1

purpose of discussion, we define the "confinement area" of the cross-section as an area containing instantaneous electric field strengths within one order of magnitude of the instantaneous maximum electric field strength. The confinement area and average field strength as a function of CPW width are shown in Fig. 1(b). As the CPW is tapered to smaller dimensions, the confinement area decreases, while the average instantaneous electric field strength increases, as expected from geometric considerations.

In order to excite THz pulses into and detect their passage through the tapered CPW, 350 nm of low-temperature-grown gallium arsenide (LT-GaAs) was epitaxially transferred onto low permittivity quartz substrates, allowing photoconductive sampling.[7] Additional steps were then necessary to complete the two different types of devices [Ti/Au tapered CPWs and giant magnetoresistance (GMR) CPWs], as now discussed.

For the Ti/Au waveguides, once the LT-GaAs was transferred, a 1 μm-wide tapered region was then defined over the LT-GaAs layer. As the dimensions of the waveguide are reduced, the device will become more sensitive to fabrication error, and therefore, the region of the narrowest taper was defined using electron-beam lithography (EBL), with the rest of the device then defined by subsequent optical lithography. Ti/Au was used for the metallisation, with thicknesses of 5 nm/70 nm for the EBL step and 5 nm/150 nm for the optical lithography step. The transition between the optical and e-beam defined metal layers was designed to be as smooth as possible by means of an overlap between the EBL and optical lithography stages to avoid impedance discontinuities.

A 100 fs pulsed laser at a centre wavelength of 800 nm was split into two paths (pump and probe). The probe path length was adjusted with a retroreflector on a motorised delay line. A symmetric bias was applied across one pair of photoconductive switches in order to excite a THz pulse propagating in the odd CPW mode. To measure the THz pulses, a lock-in amplifier was used to monitor the current generated in the ground plane when the THz pulse arrived simultaneously with the laser probe pulse. The lock-in amplifier was referenced to the frequency of an optical chopper inserted in the probe beam path. Since the ground plane was used for detection, measurements could be made anywhere along the gap between the ground plane and the centre conductor, with the exact position of measurement being determined by the location of the laser probe beam. By moving the position of the probe beam, it was thus possible to track the progress of the THz pulse as it passed through the tapered CPW [Fig. 2(a)]. The success of the smooth transition between optical and e-beam stages was verified by a lack of reflections originating from this overlap region (the small reflection signal seen in these traces originates from the far switch). Small variations in the performance of the transferred LT-GaAs were found between devices (affecting both the pulse amplitude and the signal-to-noise ratio), and it was therefore impractical to compare device attenuation directly with the HFSS modelled data. We note that the pulse shape remained consistent across all devices.

In order to demonstrate unambiguously that the THz pulse is confined to the waveguide within the highly tapered section (rather than propagating in free space or in the
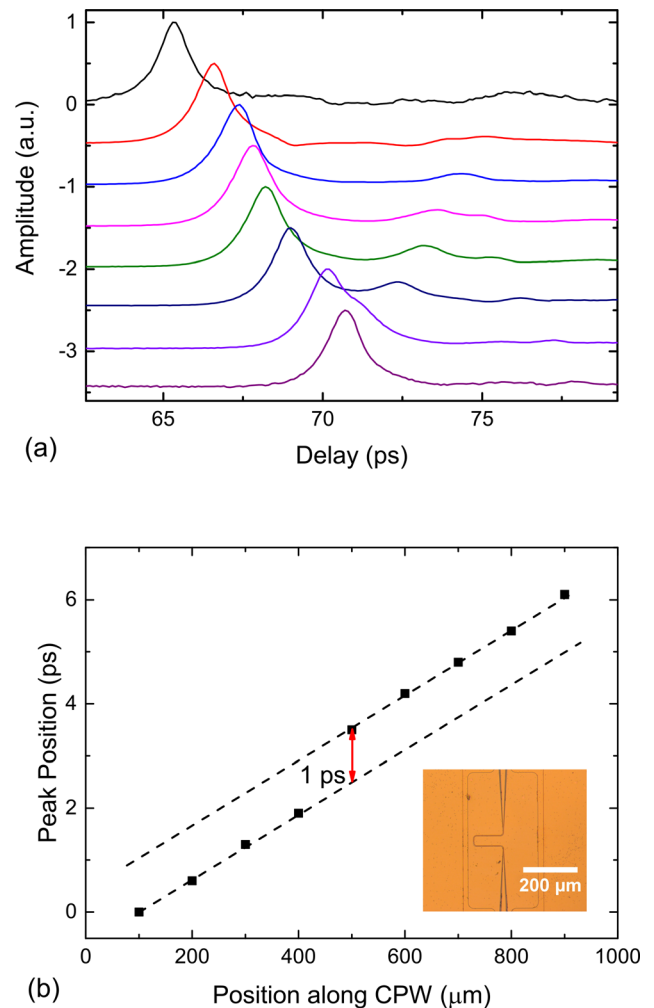
FIG. 2. (a) Normalized THz pulses measured at different positions along the tapered CPW. (b) The THz peak position for different laser probe positions along the CPW, both before (left) and after (right) propagation through an additional loop in the tapered section (inset).

dielectric), a tapered waveguide with a U-bend in the small tapered section was fabricated [inset in Fig. 2(b)]. The bend increased the transmission length by 110 μm, with the radius of curvature being 5.5 μm at the centre of the waveguide. This device was mounted on a translation stage with additional control in the z-direction. Measurements were made as described previously, but the device was then moved in 100 μm increments using the micrometer control rather than adjusting the probe beam. The pump beam was realigned after each change in the z-position. In Fig. 2(b), the position of the THz pulse peak is plotted against the measured device movement relative to its starting point. A clear jump in the THz pulse position is noted at the middle of the device, corresponding to the pulse then having to travel the increased distance through the bend section, thus confirming unambiguously that the electric field is indeed confined to the CPW even in its narrowest region. Assuming a constant pulse velocity through the entire waveguide, the extra 110 μm of CPW was expected to produce a delay of approximately 700 fs in the THz pulse arrival time. Experimentally, a delay of one picosecond was measured. This larger delay is most likely due to the effective change in the waveguide properties as the dimensions of the waveguide are reduced to a similar size to the LT-GaAs

thickness, in effect changing the substrate permittivity from that of quartz to the much higher permittivity of GaAs. This was confirmed by modelling two waveguides in HFSS, one with a centre track of width $30\,\mu m$ and the other with a centre track width of $1\,\mu m$. The effective permittivity of the waveguide at 1 THz increased from 2.6 to 5.5 with this reduction in the CPW size, respectively. The ratio of the two pulse velocities would then be $\frac{v_{30}}{v_1} = \frac{\sqrt{\epsilon_1}}{\sqrt{\epsilon_{30}}} = 1.45$, which is equal, within experimental error, to the discrepancy in the arrival times, which gives a ratio of 1.4 ± 0.1. As expected, an examination of pulse amplitudes directly before and after the U-bend reveals the extra attenuation expected from an increased propagation length. The increase in attenuation was found to be approximately $-3\,dB$ compared to a straight tapered waveguide although we note that the variability between devices may be in part responsible for this figure.

In order to quantitatively demonstrate the increase in confinement and field strength in tapered regions in practical devices, CPW devices were then made with cobalt/copper multilayers $[Co(35\,\text{Å})/Cu(10\,\text{Å})]_{\times 20}$ instead of Ti/Au.[8] For these devices, most of the transferred LT-GaAs was etched away using sulphuric acid, leaving only $70\,\mu m \times 70\,\mu m$ squares to act as photoconductive switches. Optical lithography was then used to define CPWs with six switches and two sections of the track, one section with no taper and the other with a tapered region [Fig. 3(a)]. For comparison, three waveguides were made in the same growth and with the

(a)

(b)

FIG. 3. (a) Schematic diagram showing the GMR CPW. In this example, a THz pulse is excited with the photoconductive switch pair on the left and is detected by the bottom middle switch. (b) Scaled comparison of the magnetic field response of the THz pulse amplitude for transmitted pulses through the tapered and straight sections of the CPW. The response of the tapered CPW is ~2.4 times the response of the straight section of the track. Arrows indicate the direction of the magnetic field sweep, and dashed lines are guides for the eye.

same recipe but with tapered regions where the centre conductor was reduced to $20\,\mu m$, $10\,\mu m$, and $5\,\mu m$. The dimensions of the $5\,\mu m$ waveguide were chosen as they were close to the smallest which could be achieved using optical lithography and sputtering of the multi-layered system. After metal deposition, the devices were found to exhibit a giant magnetoresistance (GMR) of 16% for DC measurements at room temperature. It has previously been shown that such changes in magnetoresistance have a direct effect on propagating THz pulses.[9]

As the waveguide dimensions reduce, our model shows that the average electric field strength in the vicinity of (loss-inducing) metal increases. Given a cross-sectional area of A and a length of L, the power dissipation in unit volume AL will be $I^2 R/(AL)$ which can be rewritten as J^2/σ using $J = I/A$ and $R = L/(A\,\sigma)$, where J is the current density, R is the resistance, and σ is the conductivity. Using Ohm's law ($J = \sigma E$), power dissipation can then be written in terms of the electric field $P = \sigma E^2$. Therefore, it is expected that the tapered region in the waveguide will induce greater dissipation due to increased field confinement. This will be discussed further below.

THz pulses were transmitted through a section of the track chosen by the position of applied bias. Pulses were measured at different magnetic fields, and a change in the pulse amplitude (but not arrival time) was noted. The delay line was then fixed so that the lock-in amplifier measured the current on the THz pulse peak continuously. The external magnetic field was then used to modify the resistance of the sample, and the change in the THz pulse amplitude with the field was measured. This was performed for both the tapered section and an adjacent straight section of CPW, for comparison. The change in THz pulse generated current as a function of external field is shown in Fig. 3(b). The GMR response in the tapered section of the waveguide is 2.4 ± 0.2 times larger than that in the straight section of the waveguide directly adjacent to it. Devices with $10\,\mu m$ and $20\,\mu m$ tapers produced experimental ratios of 1.3 ± 0.1 and 0.97 ± 0.08, respectively. "Input" pulses were also measured, where the excitation and detection switches were directly adjacent to other, separated by only ~$50\,\mu m$. In these cases, there was practically no observable change in the measured current when the magnetic field was swept.

To understand the field concentration effect, we consider the electric field in the waveguide E(x) as a function of position (x), where both attenuation and concentration will have an influence on its magnitude. To simplify the problem, E(x) is divided into components. In its simplest form, the electric field magnitude can be represented by $E(x) = E_0 e^{-\alpha x}$, where E_0 is the starting electric field magnitude and α is the attenuation constant representing all loss terms in a normal straight waveguide including ohmic, dielectric, and radiative. On application of an external magnetic field, the conductivity of the metal in the waveguide changes, and the attenuation constant will also change: $\alpha' = \alpha + \Delta\alpha$, where $\Delta\alpha$ represents the change in ohmic loss for a change in conductivity.

For a tapered waveguide, the electric field will be concentrated in the tapered region. This will increase the electric field magnitude near the loss inducing metal but not increase the

total electric field over all space. The electric field in a tapered waveguide is then $E(x) = E_0 e^{-\alpha x} e^{-\Delta \alpha x} e^{-c(x)x}(1 + E_c(x))$.

We introduce c(x) here as an additional ohmic loss term that arises from the change in waveguide geometry. It is dependent on metal resistance and thickness as well as on the degree of electric field concentration induced by the waveguide tapering. $E_c(x)$ is the increase in the electric field due to the field concentration and is defined to be zero at either end of the waveguide. In this way, the increase in the electric field magnitude is accounted for, while the only permanent aspect of the concentration is the extra attenuation.

The term $E_c(x)$ can be determined through numerical simulations (using HFSS) using a method similar to that previously described. To isolate concentration effects, however, the HFSS simulation was adjusted so that the metal was a perfect conductor and there was no substrate. Additionally, the confinement factor was reduced to two in order to examine only the strongest field in direct proximity to the metal in the waveguide. The data were similar to those shown in Fig. 1(b), and the relationship between the electric field magnitude and the waveguide width, along with the knowledge of the waveguide geometry, allowed the calculation of the field concentration for each waveguide.

The percentage change in power dissipation (%P) with changing conductivity is then considered, where $\%P = \frac{P_{max} - P_{min}}{P_{min}}$. Recalling that $P = \sigma E^2$, we then obtain

$$P_{max} = \sigma_2 \left(E_2 e^{-\alpha x} e^{-\Delta \alpha x} e^{-c(x)x}(1 + E_c(x)) \right)^2$$

and

$$P_{min} = \sigma_1 \left(E_1 e^{-\alpha x} e^{-c(x)x}(1 + E_c(x)) \right)^2,$$

where $\sigma_1 > \sigma_2$ and $\Delta \alpha$ represents the increase in α as the conductivity changes. When calculating %P, most of the terms cancel out, and %P becomes $\frac{\sigma_2 E_2^2 e^{-2\Delta \alpha x} - \sigma_1 E_1^2}{\sigma_1 E_1^2}$. From experimental measurements, it is known that the input pulse changes very little with conductivity, and therefore, from Ohm's law, $J_0 = \sigma_1 E_1 = \sigma_2 E_2$. Using this, it is found that $\%P = \frac{\sigma_1 e^{-2\Delta \alpha x} - \sigma_2}{\sigma_2}$. The change in power dissipation with conductivity in tapered and untapered waveguides can then be expressed as the ratio $R_P = \frac{P_T \%P}{P_S \%P}$, where P_T and P_S represent the total power dissipation in the tapered and straight sections of the waveguide, respectively. Since %P cancels, this ratio only depends on these total power dissipation values. The total power dissipation in the straight waveguide is then $P_S = \int_0^1 \sigma E^2(x)dx = \sigma \overline{E^2(x)}$, where $\overline{E^2(x)}$ is the mean value of the electric field squared. Using the mean value simplifies the problem considerably, and this strategy can also be used for P_T. For the purposes of calculating power dissipation, the x dependence of $E_c(x)$ can be removed and replaced with the mean value of $E_c(x)$ in the waveguide. In this way, we can get E_c and $E_{c,sq}^2$, where $E_c = \overline{E_c(x)}$ and $E_{c,sq}^2 = \overline{E_c^2(x)}$. Note here that $E_c \neq \sqrt{E_{c,sq}^2}$.

Since power dissipation is responsible for the extra attenuation in the tapered region, it is also possible to express c(x) in terms of E_c. This becomes $c(x) = k\sqrt{E_{c,sq}^2}$, where k is a parameter that varies with metal properties and thickness. When considering the three devices made with the same recipe, however, it can be viewed as a constant.

The ratio R_P then becomes $\frac{\sigma_1 (E_1 e^{-\alpha x} e^{-k\sqrt{E_{c,sq}^2}}(1 + E_c(x)))^2}{\sigma_1 (E_1 e^{-\alpha x})^2}$ $= e^{-2k\sqrt{E_{c,sq}^2}}(1 + 2E_c + E_{c,sq}^2)$. However, since it is current, and not power dissipation that is being measured, the square root needs to be calculated in order to compare with the experimental data. The ratio of current change in tapered and untapered waveguides is then $R_J = \sqrt{e^{-2k\sqrt{E_{c,sq}^2}}(1 + 2E_c + E_{c,sq}^2)}$, where only k is unknown. Numerically solving R_J for a range of k values reveals that for k = 0.01, the ratio is equal to 2.2, 1.4, and 1.06 for 5 μm, 10 μm, and 20 μm tapers, respectively, corresponding well to the experimental results of 2.4 ± 0.2, 1.3 ± 0.1, and 0.97 ± 0.08. Our analysis showed that the 1 μm taper waveguides studied would show an enhancement ratio of 2.8, while tapering to smaller dimensions would result in larger enhancement factors, consistent with the increased field concentration shown in Fig. 1(b).

In conclusion, we have measured the time domain response of tapered on-chip coplanar THz waveguides with integrated photoconductors. Confinement to the waveguide in the narrowest sections of CPW was demonstrated by transmitting a THz pulse through a U-bend to delay the signal. Increased field confinement in tapered waveguides formed from materials exhibiting GMR was also demonstrated. Tapered waveguides provide significant potential for studying the picosecond response of individual micron length-scale objects and systems, with the attendant field concentration potentially allowing non-linear effects to be accessed.

[1]R. Layman, A. Gorodetsky, N. Bazieva, G. Molis, A. Krotkus, E. Clarke, and E. U. Rafailov, Laser Photonics Rev. **10**(5), 772 (2016).
[2]P. Dean, O. Mitrofanov, J. Keeley, I. Kundu, L. Li, E. H. Linfield, and A. G. Davies, Appl. Phys. Lett. **108**, 091113 (2016).
[3]O. Mitrofanov, I. Khromova, T. Siday, R. J. Thompson, A. N. Ponomarev, I. Brenar, and J. L. Reno, IEEE Trans. THz Sci. Technol. **6**, 382 (2016).
[4]J. Wu, A. S. Mayorov, C. D. Wood, D. Mistry, L. Li, W. Muchenje, M. Rosamond, L. Chen, E. H. Linfield, A. G. Davies, and J. E. Cunningham, Sci. Rep. **5**, 15420 (2015).
[5]J. Wu, O. Sydoruk, A. S. Mayorov, C. D. Wood, D. Mistry, L. Li, E. H. Linfield, A. G. Davies, and J. E. Cunningham, Appl. Phys. Lett. **108**, 091109 (2016).
[6]*HFSS v15, Release 15.0.7* (Ansys Inc, Pittsburg, PA, 2014).
[7]M. Swithenbank, A. D. Burnett, C. Russell, L. H. Li, A. G. Davies, E. H. Linfield, J. E. Cunningham, and C. D. Wood, Anal. Chem. **89**(15), 7981–7987 (2017).
[8]S. S. P. Parkin, R. Bhadra, and K. P. Roche, Phys. Rev. Lett. **66**, 2152 (1991).
[9]Z. Jin, A. Tkach, F. Casper, V. Spetter, H. Grimm, A. Thomas, T. Kampfrath, M. Bonn, M. Kläui, and D. Turchinovich, Nat. Phys. **11**(9), 761 (2015).